JOURNAL OF SOLID STATE CHEMISTRY 120, 268–274 (1995)

Oxidation Products of $Nb_4W_{13}O_{47}$: A Transmission Electron Microscopy Study

F. Krumeich[1]

Institut für anorganische Chemie der Universität Bonn, Römerstrasse 164, D-53117 Bonn, Germany

and

C. Bartsch and R. Gruehn

Institut für anorganische und analytische Chemie der Universität Gießen, Heinrich-Buff-Ring 58, D-35392 Giessen, Germany

Received April 19, 1995; accepted July 19, 1995

$Nb_4W_{13}O_{47}$, a mixed valency oxide crystallizing in the structure of the 4:9 phase ($4Nb_2O_5 \cdot 9WO_3$), was oxidized at various temperatures. The products have been characterized by high-resolution transmission electron microscopy. Oxidation products obtained at 600 and 1000°C exhibit the development of planar defects running along {110} of the TTB subcell. The defects are built up by structural elements observed here for the first time: Two or more five-membered rings of octahedra are connected via two common octahedra. These arrays are combined with blocks of ReO_3-type structure and ordered along the defect planes. The oxidation at 1200°C leads to a separation into the 2:7 phase and WO_3.

1. INTRODUCTION

In the pseudo-binary Nb_2O_5/WO_3 system, the so-called 4:9 phase ($4Nb_2O_5 \cdot 9WO_3 \equiv Nb_8W_9O_{47}$) represents the most stable compound (1). It crystallizes in a threefold superstructure of the tetragonal tungsten bronzes (TTB) originating from a systematic distribution of PCs (pentagonal columns (2, 3)) as shown in Fig. 1a. Furthermore, the oxide $Nb_8W_9O_{47}$ can be regarded as the end member ($n = 0$) of a solid solution series $Nb_{8-n}W_{9+n}O_{47}$ ($0 < n \leq 5$) in which Nb^{5+} is substituted by Nb^{4+} or W^{4+}, respectively, and W^{6+} (4). Starting from oxides with $n > 0$, metastable products with an increasing $O/\Sigma M$ ratio become accessible by oxidation of the incompletely oxidized portion of cations (5). The composition of the products lies in between those of $(Nb,W)O_{2.7647}$ ($Nb_8W_9O_{47}$) and WO_3. In this region of the system Nb_2O_5/WO_3, three intergrowth phases between the TTB- and ReO_3-type structure have been observed (6, 7), but only the 2:7 phase (Fig. 1b) seems to be thermodynamically stable (8). In addition, Magnéli phases exist for $O/\Sigma M > 2.9$ (9).

An investigation of the oxidation products of $Nb_7W_{10}O_{47}$ ($n = 1$) was performed recently (10). Depending on the oxidation temperature, several structural possibilities of accommodating the oxygen excess were observed. The cation sites of the developed structures were detected by HRTEM (high-resolution transmission electron microscopy). This method is a very useful tool for exploring the structure of aperiodic defects in TTB-type compounds. Since the polyhedra are always connected by corner-sharing along the *c*-axis, metal–oxygen strings occur which can be imaged as dark dots in projection onto the *a*–*b*-plane (4, 11).

In the present contribution, we describe the results of similar oxidation experiments carried out on $Nb_4W_{13}O_{47}$ ($n = 4$). This member of the solid solution series has a higher number of cations in a lower oxidation state than $Nb_7W_{10}O_{47}$. Therefore, oxidation according to

$$Nb_4W_{13}O_{47} + O_2 = Nb_4W_{13}O_{49}$$

leads to products with a much higher $O/\Sigma M$ ratio (2.882) compared with oxidized $Nb_7W_{10}O_{47}$ ($O/\Sigma M = 2.794$). In connection with the increased W/Nb ratio (13:4 > 10:7 in $Nb_7W_{10}O_{47}$) deviating phase relationships are expected.

2. EXPERIMENTAL

Preparation

Samples with the appropriate composition $Nb_4W_{13}O_{47}$ were prepared by two different routes: Mixtures of Nb_2O_5,

[1] Present address: Institut für Angewandte Chemie Berlin Adlershof, Rudower Chaussee 5, D-12484 Berlin, Germany.

0022-4596/95 $12.00

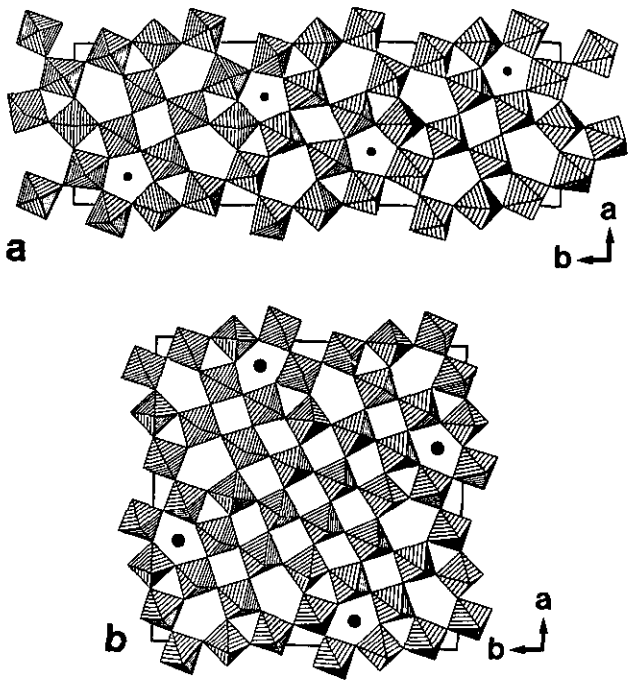

FIG. 1. Structure models of (a) 4:9 phase [2] and (b) 2:7 phase [6].

WO_3 (both puriss., Fluka AG), and WO_2 in the ratio 2:9:4 or WO_3 and NbO_2 in the ratio 13:4 were made. NbO_2 and WO_2 were prepared by reduction of Nb_2O_5 and WO_3, respectively, with metal foils (12). $Nb_4W_{13}O_{47}$ was obtained as a dark blue crystalline product by annealing (1250°C; 3*d*) the mixtures with 4 mg $HgCl_2$ (mineralizer) in an evacuated silica ampoule (4). The products are identical for both routes as shown by X-ray powder diffraction (Guinier method, $\lambda = 0.15405$ nm) and transmission electron microscopy. The lattice parameters of the orthorhombic unit cell are: $a = 1.225$, $b = 3.659$, and $c = 0.3897$ nm (4). The oxidation reaction (on air) was performed independently with ground material of $Nb_4W_{13}O_{47}$ at 600°C; 1*d* (sample I), 1000°C; 3*d* (II), and 1200°C; 2*d* (III).

Electron Microscopy

The samples were crushed and dispersed onto holey films (carbon coated Formvar) supported on copper grids. The electron diffraction and HRTEM investigation was performed using Philips CM30ST microscopes operated at 300 kV (LaB_6 cathode). Thin crystal flakes were orientated along the short crystallographic axis [001] to observe the crystal structure in projection onto the *a*–*b*-plane.

3. RESULTS AND DISCUSSION

3.1. Oxidation at 600 and 1000°C

Oxidation at low temperature (T_{ox} = 600°C; sample I) already leads to structural changes similar to those observed in the case of higher temperature (T_{OX} = 1000°C;

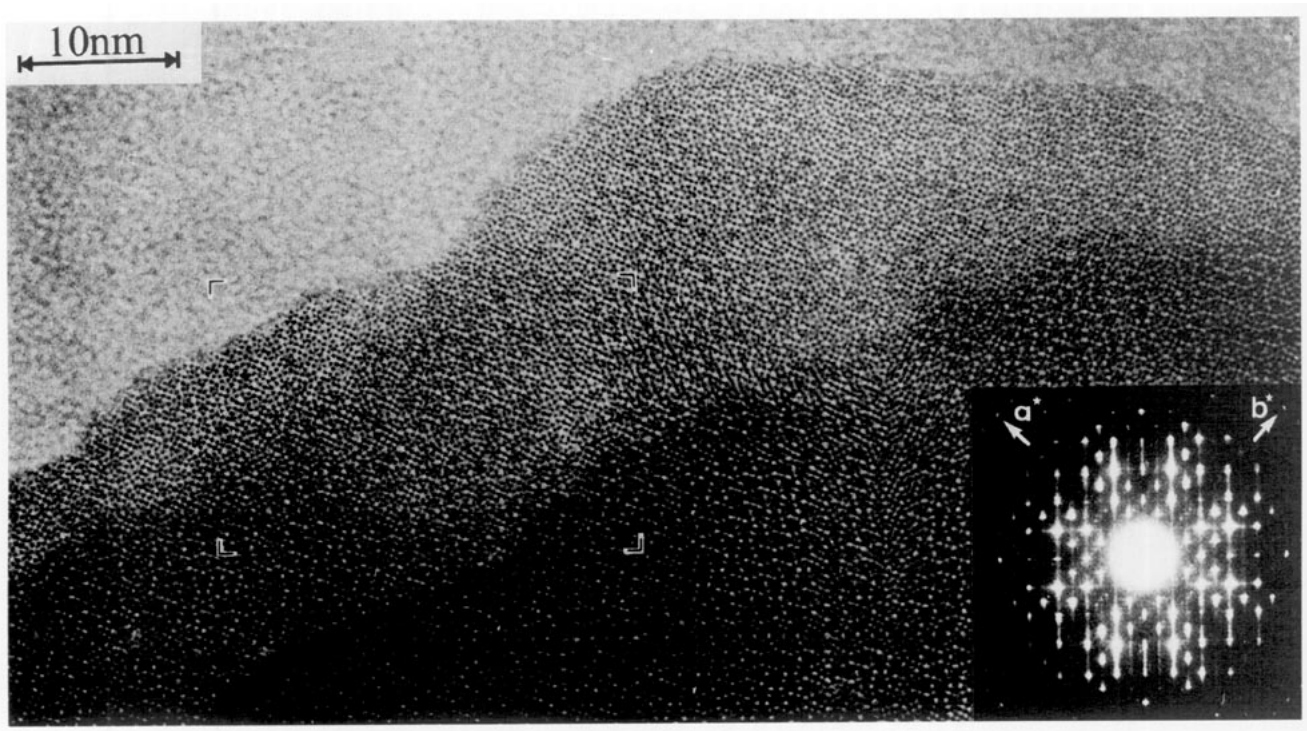

FIG. 2. HRTEM image of $Nb_4W_{13}O_{49}$ (T_{ox} = 600°C; sample I). The inset shows the electron diffraction pattern. The area limited by four corners shows the enlargement represented in Fig. 3.

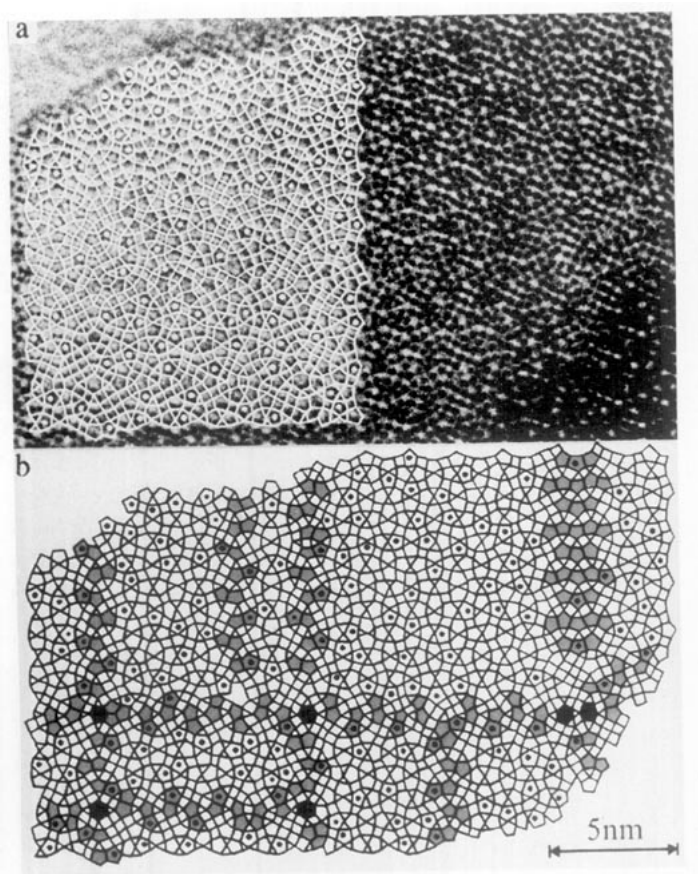

FIG. 3. (a) Enlarged area of Fig. 2 and (b) interpretation. For easier interpretation of the observed defect structures a simplified way of representation is chosen: Dark dots in the lattice images corresponding to octahedral cation sites were connected by lines, whereas the cations located in pentagonal tunnels are indicated by filled circles. The image in (a) is partially superimposed by this scheme.

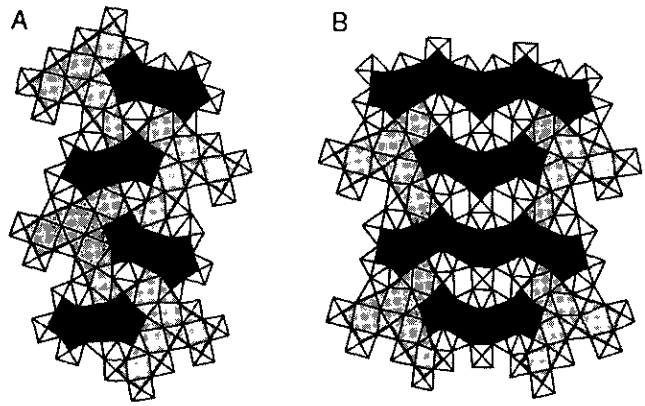

FIG. 5. Structure models of unit A and unit B.

sample II). This is indicated by the similarity of the electron diffraction patterns (insets in Figs. 2 and 4): The reflections of the threefold superstructure disappeared, only those of the TTB subcell remain. In both cases, the orientation relationship between the orthorhombic superstructure and the remaining tetragonal substructure is not recognizable. Additional streaks occur along $\langle 110 \rangle^*$, indicating stacking disorder. The structural origin of these features becomes obvious from lattice images (Figs. 2–4). Planar defects appear along two perpendicular directions ([110] and $[1\bar{1}0]$ of the TTB subcell) between microdomains with TTB structure, in which the distribution of PCs is disordered.

The structure of the defects consists of structural elements observed here for the first time. Two or more five-membered rings (pentagons) of MO_6 octahedra are con-

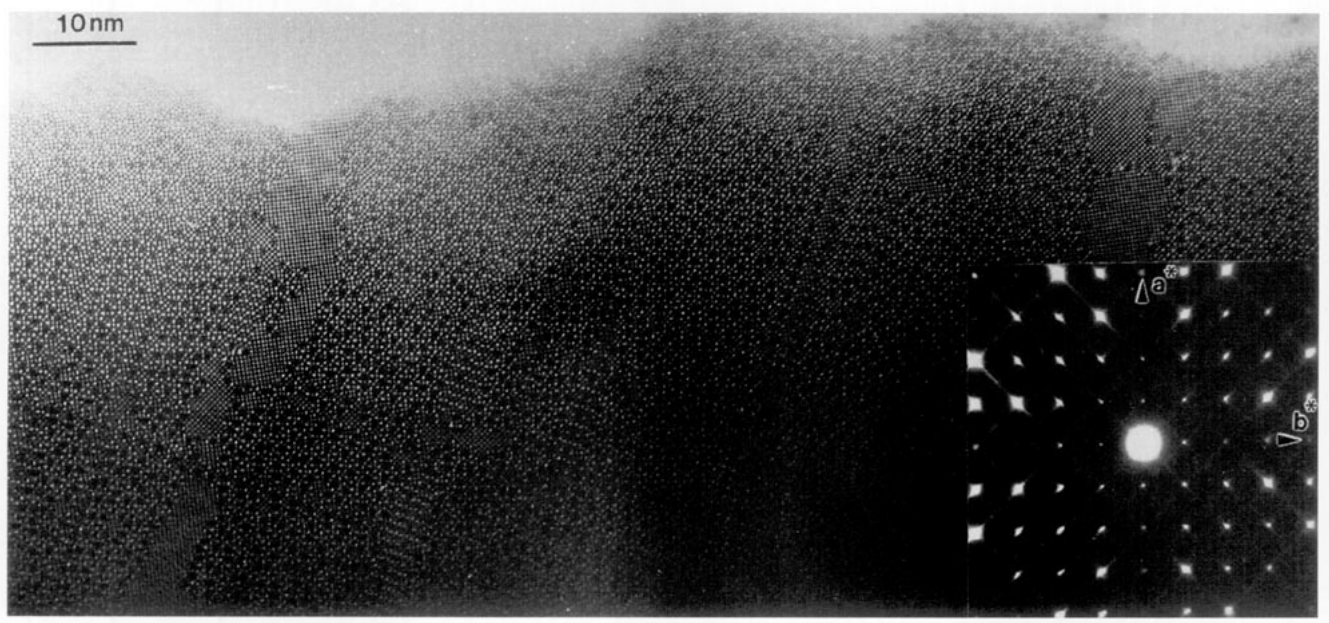

FIG. 4. HRTEM image of $Nb_4W_{13}O_{49}$ (T_{ox} = 1000°C; sample II). The inset shows the electron diffraction pattern.

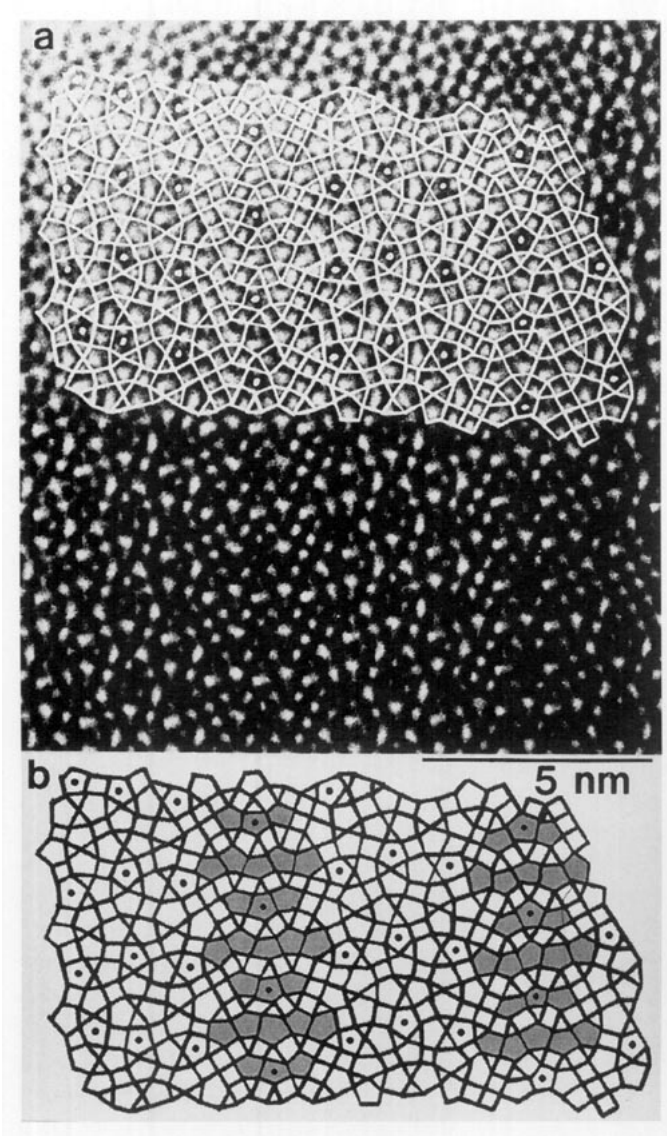

FIG. 6. (a) Enlarged area (sample II) showing lines of unit B and (b) interpretation. P_n's are shaded.

nected by edge-sharing. For simplification, we introduce the symbol P_n with subscript n indicating the number of combined pentagons. P_n's are always adjoined to small arrays of ReO_3-type structure. Mainly, two different structural units (A and B, Fig. 5) were formed which are arranged along the planar defects in an ordered way. Unit A consists of two pentagonal rings joined by edge-sharing, resulting in a pair of pentagons (P_2). This type of linkage between five-membered rings of octahedra has been observed before in defects of tungsten-rich $(Nb,W)O_{2.925}$ (13) and of oxidized $W_{18}O_{49}$ (14, 15). In unit A, the P_2's are connected to form an arrangement of five squares of corner-sharing octahedra having the shape of a T. The resulting units group themselves into zigzag chains with the P_2's located alternately on the left or right (A in Fig. 5). This feature is predominant in the case of sample I (Figs. 2, 3). The P_2's are not occupied with metal–oxygen strings in a ordered manner but the pentagons facing the center of the region always remain empty. The defects are oriented along two perpendicular directions ([110] and $[1\bar{1}0]$) and intersect each other in several places. At the crossings, six-membered rings of octahedra are formed (Fig. 3).

In unit B, rows of threefold and fivefold pentagons (connected by edge-sharing) are ordered alternately (Fig. 5). The P_3's are linked on both ends to a T formed by squares of octahedra. Arrangements of unit B appear ordered in many areas (Fig. 6). Obviously, each central pentagonal tunnel of the P_3's is occupied. The units are arranged in two parallel lines, but their structures are rotated 180° with respect to each other. The TTB framework between them,

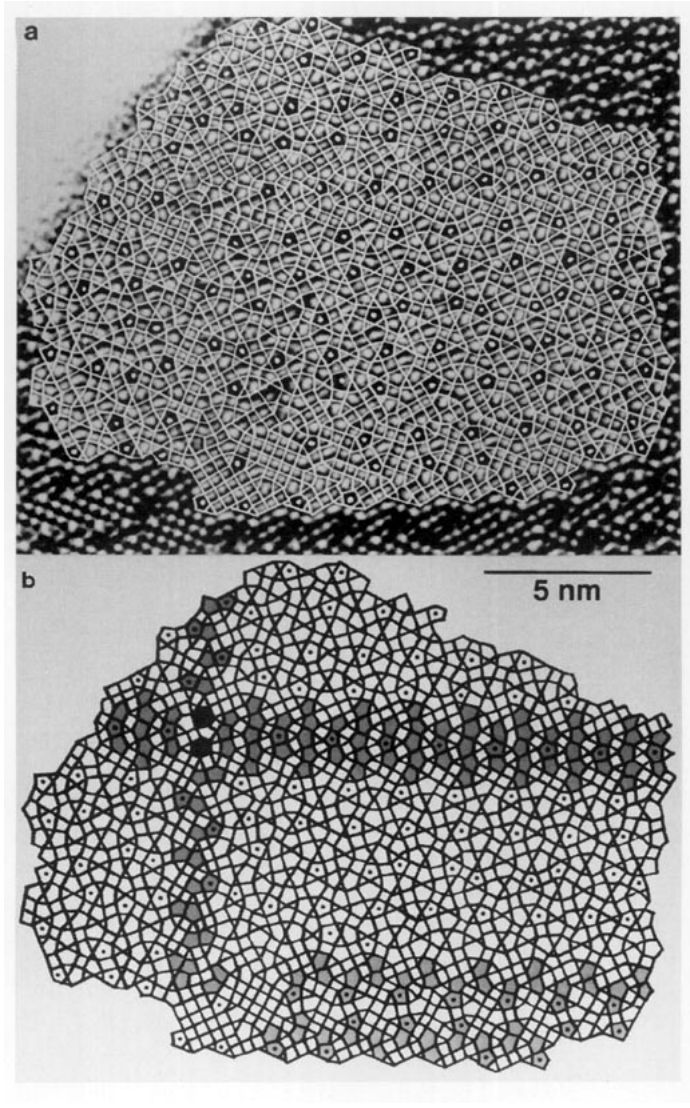

FIG. 7. (a) Enlarged area (sample II) showing a special connection of A units and (b) interpretation.

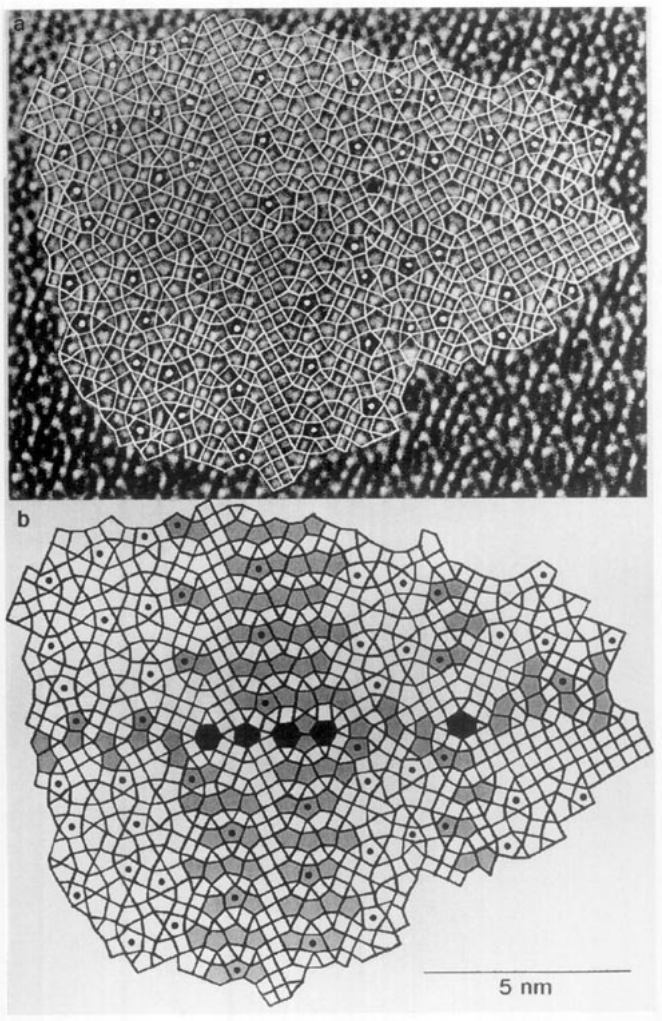

FIG. 8. (a) Enlarged area (sample II) and (b) interpretation. Four hexagons (black) appear at the intersection of a line of unit A and a more complicated defect.

as well as on both sides, is undisturbed and fits coherentely onto the defect.

Lines of both structural units (A, B) are present in the crystal area shown in Fig. 7. They are oriented perpendicular to each other. At their intersection, two hexagons appear. Furthermore, arrangements are recognizable which exhibit more complicated structures. In the lower part of Fig. 7, two lines of units A are oriented antiparallel, linked by two Ts which have a square of octahedra in common. This leads to the inclusion of single units of the TTB structure into the defect. These are almost surrounded by squares of octahedra forming double Ts. Two of the four pentagonal tunnels in the TTB unit, which are filled with metal–oxygen strings in most cases, are connected with others to forming P_2's. At one end of this defect (left side of Fig. 7), larger blocks with ReO_3-type structure appear. These probably consist of WO_3, as was shown using EDX analysis for similiar segregations in a sample of $Nb_7W_{10}O_{47}$ obtained by oxidation (T_{ox} = 1000°C) (10).

Other types of defects, occurring in the crystal area shown in Fig. 8, are complicated variants of the two basic structural units (A, B). At the lower part of the defect in the center of Fig. 8, two lines of slightly modified B units are combined in antiparallel orientation (PCs in the center of P_3's point in opposite directions). A slab with ReO_3-type structure separates the lines formed by alternating groups of P_3's and P_5's. Compared to unit B, this arrangement is different since one pentagon of the P_5's has vanished. A similar arrangement is recognizable in the perpendicular direction, where it is connected to a broader ReO_3 slab (right side of Fig. 8). At the crossing with a defect formed by A units, four hexagons are located. The slabs with ReO_3-type structure slip at the crossing so that another type of defect structure appears on the other side. On the left side of the ReO_3 slab, P_2's, Ts of octahedra squares, and single pentagonal tunnels are present. This arrangement is closely related to that of unit A but in every second P_2 one pentagonal tunnel is absent. On the other side of the slab, P_5's and P_6's are ordered in alternating rows. A T terminates the P_5's. As usual, the defect regions are enclosed coherently in the TTB framework. The distribution of occupied pentagonal tunnels is disordered in the whole area.

Besides planar defects, the appearance of extended areas of segregated WO_3 (Fig. 4) is a characteristic of sample II (T_{ox} = 1000°C). Furthermore, crystals (not shown here) have been observed where the oxidation led to the separation of single units of the 2:7 phase (Fig. 1b) which has a higher tungsten content. These are embedded in a TTB framework which exhibits a disordered distribution of the PCs. These crystals are similar to that observed for $Nb_7W_{10}O_{47}$ oxidized at 1200°C (10).

3.2. *Oxidation at 1200°C*

The oxidation of $Nb_4W_{13}O_{47}$ at 1200°C leads to a phase separation mainly into the 2:7 phase (Fig. 1b) and WO_3. This is already obvious from the electron diffraction pattern (inset in Fig. 9). The tetragonal unit cell of the 2:7 phase has an *a*-axis twice of that of the TTB cell. Therefore, it is recognizable in the *a*–*b*-plane because of the superstructure reflections. The very intense reflections correspond to the ReO_3-type structure. Two different sets of them are present indicating two distinct orientation relationships between the TTB-type matrix structure and the ReO_3-type segregations as confirmed by lattice imaging (Fig. 9). As one can easily recognize by the presence of 4×4 blocks of octahedra (3×3 bright dots), the 2:7 type is predominant in the lower left area of the micrograph. This area is surrounded by large segregations of WO_3. Numerous TTB cells are incorporated into the ReO_3-type

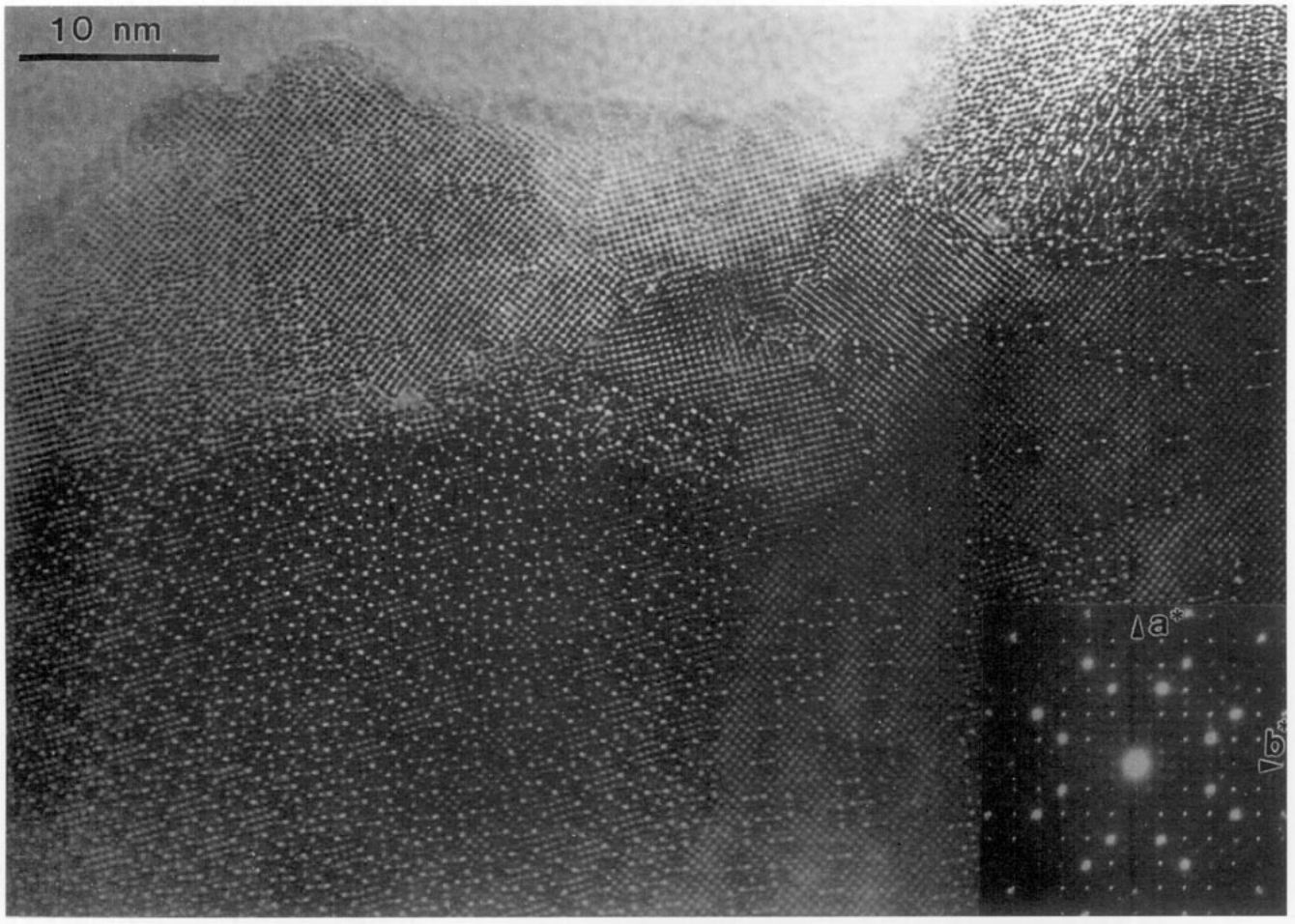

FIG. 9. HRTEM image of $Nb_4W_{13}O_{49}$ (T_{ox} = 1200°C; sample III). The inset shows the electron diffraction pattern.

structure; furthermore, some of them are found among the 2:7 units. Domains of WO_3, which are tilted with respect to each other, are separated by boundaries with pentagonal tunnels. Similiar intergrowths of ReO_3- and TTB-type structures had been already observed in niobium tungsten oxides obtained by solid state reaction of the binary oxides. Iijima and Allpress (6) discussed these structures in detail.

4. CONCLUSIONS

The complete oxidation of $Nb_4W_{13}O_{47}$ leads to a composition $Nb_4W_{13}O_{49}$ which is, concerning its $O/\Sigma M$ ratio of 2.882, located in between the 2:7 phase (2.818) and WO_3 (Fig. 10). The corresponding phase separation according to

$$Nb_4W_{13}O_{49} = Nb_4W_7O_{31} + 6\ WO_3$$

is only observed after oxidation at 1200°C. At lower oxidation temperatures, the segregation of the 2:7 phase does not occur completely; only single columns of unit cells have been observed in some crystals oxidized at 1000°C. Instead, metastable products develop preferentially. Similar oxidation experiments performed on $Nb_7W_{10}O_{47}$ led to analogous results (10) concerning the phase relationships: The expected separation into 4:9 and 2:7 phases (Fig. 10) was only observed at 1200°C, whereas at lower oxidation temperature WO_3 is segregated instead of the 2:7 phase. Therefore, we are able to confirm the conclusion of Roth and Waring (8) that the area of existence of the 2:7 phase is limited at temperature above 1000°C.

By oxidation of niobium tungsten oxides $(Nb,W)_{17}O_{47}$ with mixed valency, tungsten-rich products can be prepared at relatively low temperatures. If high oxidation temperatures (1200°C) are applied, the products are similiar, concerning their structures, to those obtained by solid state reactions between Nb_2O_5 and WO_3. On the other hand, oxidation at low temperatures ($\leq$1000°C) provides a route to products exhibiting interesting new structural features.

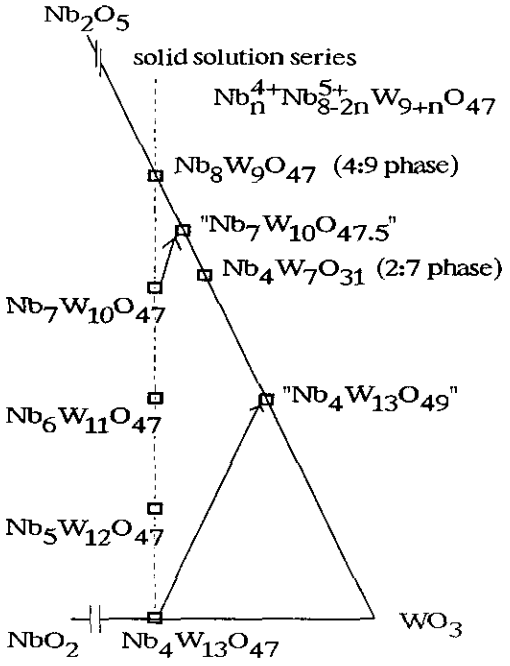

FIG. 10. Part of the phase diagram $NbO_2/Nb_2O_5/WO_3$ (simplified). The phase shifts caused by the nonequilibrium oxidation reaction are indicated by arrows. For "$Nb_7W_{10}O_{47}$" see (10). Magnéli phases ($O/\Sigma M > 2.9$) [9] are omitted.

ACKNOWLEDGMENTS

We gratefully acknowledge Prof. Dr. A. Hussain for providing the source material $Nb_4W_{13}O_{47}$. This study was supported by the Deutsche Forschungsgemeinschaft and the Fonds der Chemie.

REFERENCES

1. M. W. Viccary and R. J. D. Tilley, *J. Solid State Chem.* **104,** 131 (1993).
2. A. W. Sleight, *Acta Chem. Scand.* **20,** 1102 (1966).
3. B.-O. Marinder, *Angew. Chem., Int. Ed. Engl.* **25,** 431 (1986).
4. F. Krumeich, A. Hussain, C. Bartsch, and R. Gruehn, *Z. Anorg. Allg. Chem* **621,** 799 (1995).
5. F. Krumeich, C. Bartsch, A. Hussain, and R. Gruehn, *in* "7. Vortragstagung der Fachgruppe Festkörperchemie, Bonn," PO I 35, 1994.
6. S. Iijima and J. G. Allpress, *Acta Crystallogr. Sect. A* **30,** 22 (1974).
7. S. Iijima, *Acta Crystallogr. Sect. A* **34,** 922 (1978).
8. R. S. Roth and J. L. Waring, *J. Res. Natl. Bur. Stand. Sect. A* **70,** 281 (1966).
9. P. J. England, J. Booth, R. J. D. Tilley, and T. Ekström, *J. Solid State Chem.* **44,** 60 (1982).
10. F. Krumeich, *J. Solid State Chem.* **119,** 420 (1995).
11. S. Horiuchi, K. Muramatsu, and Y. Matsui, *Acta Crystallogr. Sect. A* **34,** 939 (1978).
12. A. Hussain, B. Reitz, and R. Gruehn, *Z. Anorg. Allg. Chem.* **535,** 186 (1986).
13. P. J. England and R. J. D. Tilley, *Chem. Scr.,* **20,** 102 (1982).
14. W. Sahle, *J. Solid State Chem.* **45,** 324 (1982).
15. W. Sahle, *Chem. Commun. Univ. Stockholm,* **4** (1983).